THE ASTROPHYSICAL JOURNAL, 184:605–631, 1973 September 1

STRUCTURE OF THE SOLAR CHROMOSPHERE. I. BASIC COMPUTATIONS AND SUMMARY OF THE RESULTS

JORGE E. VERNAZZA
Harvard College Observatory, Cambridge, Massachusetts
AND
EUGENE H. AVRETT AND RUDOLF LOESER
Smithsonian Astrophysical Observatory, Cambridge, Massachusetts
Received 1973 February 12; revised 1973 April 27

ABSTRACT

We compute a one-component model of the solar atmosphere, including in that model the photosphere, chromosphere, and chromosphere-corona transition zone. The calculations are performed with PANDORA, a general computer program that enables us to obtain detailed solutions of the radiative-transfer and statistical-equilibrium equations for a six-level hydrogen atom and for eight-level C I and Si I atoms. All radiative transitions are treated explicitly. The program is formulated in a general way and is currently being used for the analysis of other atomic systems as well. The present calculation of the continuous absorption and emission throughout the spectrum takes into account the non–LTE contributions of H, H^-, C I, and Si I. Other ions and atoms are treated in LTE. The atmosphere is assumed to be in hydrostatic equilibrium, but radiative equilibrium is not assumed. By trial-and-error adjustments, we obtained an empirical temperature-height distribution such that our computed synthetic intensities are consistent with the observed radiation from the chromosphere in the extreme-ultraviolet and microwave regions of the quiet solar spectrum.

Our present determination of chromospheric structure differs from previous ones in that the Lyman lines are treated explicitly; they are not assumed to be in detailed balance. We find that small departures from detailed balance in the Lyman lines can lead to significant changes in the ionization of hydrogen in the middle chromosphere.

The present paper is concerned mainly with the equations we solve in order to construct the solar model. Section XI gives a brief summary of the results. Further details will appear in subsequent papers of this series.

Subject headings: atmospheres, solar — chromosphere, solar — spectra, solar

I. INTRODUCTION

In most astrophysical problems, the physical properties of a radiating plasma can be inferred by means of spectroscopic observations. The interpretation of these observations becomes difficult when (1) the plasma is optically thick and (2) local thermodynamic equilibrium (LTE) cannot be assumed. In this paper, we describe the mathematical basis of a computer program, called PANDORA, for calculating the level populations and the radiation field for various atoms in an optically thick, non-LTE plasma that has a given temperature structure. We assume hydrostatic equilibrium in order to determine the corresponding density structure.

We have used PANDORA to construct a detailed model of the solar chromosphere. While the program can be used to calculate models of any star, the Sun has been chosen because of the existence of a large amount of observational data, particularly at ultraviolet wavelengths, where the spectrum originates at various chromospheric heights. Our chromospheric model is an empirical one, determined by adjusting the temperature as a function of height to that distribution that gives best agreement between the synthesized continuous spectrum and the corresponding observed spectrum

and, to a lesser extent, between synthesized and observed line spectra. We attempt in this way to construct the best possible one-component model of the quiet solar chromosphere—representing an average over small-scale inhomogeneities. One-component models are not consistent with the center-to-limb behavior of certain strong lines and continua formed high in the chromosphere, so we have based our model on observations at the center of the solar disk.

The present paper is devoted almost entirely to a description of the equations we solve in order to determine a theoretical model. In subsequent papers, we will present detailed solutions for each of the atomic systems studied.

Section XI summarizes the results of the model calculation and shows how the predicted intensities agree with solar observations. In the concluding section, we outline the present status of our research and its direction for the near future.

Those interested primarily in our results may wish to read these last two sections first and to regard the mathematical development given in §§ II–X as background reference material.

II. STATISTICAL EQUILIBRIUM EQUATIONS

We describe here the calculation of atomic number densities and departure coefficients in terms of specified line and continuum radiation fields. This section contains a more explicit development of equations than do other sections, because we feel that this material has not been published elsewhere in sufficient detail.

Consider an atom with $\mathcal{N}$ bound levels and one higher stage of ionization; the equation of statistical equilibrium for level l is

$$n_l\left(\sum_{m=1(\neq l)}^{\mathcal{N}} P_{lm} + P_{l\kappa}\right) = \sum_{m=1(\neq l)}^{\mathcal{N}} n_m P_{ml} + n_\kappa P_{\kappa l}\,, \tag{1}$$

where n_l and n_m are the bound-level number densities, n_κ is the number density of ionized atoms, and P_{ij} is the i to j transition rate per atom in the initial state. We also require

$$\sum_{l=1}^{\mathcal{N}} n_l + n_\kappa = n_{\text{total}}\,. \tag{2}$$

Given the various rate coefficients and the total number density of the two stages of ionization, the linear set of equations (1) for $l = 1, 2, \ldots, \mathcal{N}$ together with equation (2) can be used to solve for all the number densities.

These equations can be written in another, more convenient form in which n_κ does not appear. The sum of equations (1) for $l = 1, 2, \ldots, \mathcal{N}$ is the continuum equation

$$n_\kappa \sum_{l=1}^{\mathcal{N}} P_{\kappa l} = \sum_{l=1}^{\mathcal{N}} n_l P_{l\kappa}\,. \tag{3}$$

Using this result to eliminate n_κ from equation (1), we get

$$n_l \sum_{m=1(\neq l)}^{\mathcal{N}} (P_{lm} + \mathcal{P}_{lm}) = \sum_{m=1(\neq l)}^{\mathcal{N}} n_m (P_{ml} + \mathcal{P}_{ml})\,, \tag{4}$$

where $\mathcal{P}_{ij}$ is given by

$$\mathcal{P}_{ij} = P_{i\kappa} P_{\kappa j} \Big/ \sum_{l=1}^{\mathcal{N}} P_{\kappa l} \tag{5}$$

and represents the indirect rate from i to j through the continuum. As explained later, we use equation (4) to obtain ratios of the bound-level number densities (or ratios of the equivalent departure coefficients b_l) from given values of P_{ij} and $\mathscr{P}_{ij}$.

Let us now consider the bound-free rates appearing in equations (3) and (5). These rate coefficients can be written as

$$P_{l\kappa} = R_{l\kappa} + C_{l\kappa} \tag{6}$$

and

$$P_{\kappa l} = R_{\kappa l} + C_{\kappa l} , \tag{7}$$

where the photoionization rate is

$$R_{l\kappa} = 4\pi \int_{\nu\kappa_l}^{\infty} \frac{1}{h\nu} \alpha_l(\nu) J_\nu d\nu , \tag{8}$$

and the radiative recombination rate (per ionized atom) is

$$R_{\kappa l} = \frac{n_l^*}{n_\kappa^*} R_{l\kappa}^\dagger , \tag{9}$$

where

$$R_{l\kappa}^\dagger = 4\pi \int_{\nu\kappa_l}^{\infty} \frac{1}{h\nu} \alpha_l(\nu) e^{-h\nu/kT} \left(\frac{2h\nu^3}{c^2} + J_\nu \right) d\nu . \tag{10}$$

We note that $R_{l\kappa}^\dagger = R_{l\kappa}$ when J_ν is the Planck function. The thermodynamic-equilibrium ratio n_l^*/n_κ^* is given by the Saha-Boltzmann equation

$$\frac{n_l^*}{n_\kappa^*} = n_e \left(\frac{h^2}{2\pi mkT} \right)^{3/2} \frac{\varpi_l}{2U_\kappa} \exp\left(h\nu_{\kappa l}/kT\right) , \tag{11}$$

where ϖ_l is the statistical weight of level l and U_κ is the partition function for the next stage of ionization. The other symbols have their usual meaning. Since the collisional ionization and recombination rates satisfy

$$C_{\kappa l} = \frac{n_l^*}{n_\kappa^*} C_{l\kappa} , \tag{12}$$

we can write

$$P_{\kappa l} = \frac{n_l^*}{n_\kappa^*} P_{l\kappa}^\dagger , \tag{13}$$

where

$$P_{l\kappa}^\dagger = R_{l\kappa}^\dagger + C_{l\kappa} . \tag{14}$$

We define the departure coefficient b_l for level l according to

$$n_l = b_l n_\kappa n_l^*/n_\kappa^* . \tag{15}$$

This definition is equivalent to the one first introduced by Menzel (1937) and is now, in effect, the customary one. It implies that $b_\kappa \equiv 1$ and that

$$b_l = \frac{n_l/n_l^*}{n_\kappa/n_\kappa^*} . \tag{16}$$

Often b_l differs from unity mainly because $n_\kappa \neq n_\kappa^*$. However, this complication, involving the degree of ionization, is not present in the ratio of departure coefficients:

$$\frac{b_l}{b_m} = \frac{n_l/n_l^*}{n_m/n_m^*} = \frac{n_l/n_m}{n_l^*/n_m^*} . \tag{17}$$

From equation (11), the ratio n_l^*/n_m^* is given by the Boltzmann equation

$$\frac{n_l^*}{n_m^*} = \frac{\varpi_l}{\varpi_m} \exp(-h\nu_{lm}/kT) , \qquad l > m . \tag{18}$$

Now we return to equations (2) and (3) to obtain expressions for b_l and n_l in terms of the ratios b_l/b_m. The continuum equation (3) can be written

$$\sum_{l=1}^{\mathcal{N}} \frac{n_l^*}{n_\kappa^*} P_{l\kappa}^{\dagger} = \sum_{l=1}^{\mathcal{N}} b_l \frac{n_l^*}{n_\kappa^*} P_{l\kappa} . \tag{19}$$

We divide both sides of this equation by $\varpi_1 n_1^*/n_\kappa^*$ and define $Q_{l\kappa} = \gamma_l P_{l\kappa}$ and $Q_{l\kappa}^{\dagger} = \gamma_l P_{l\kappa}^{\dagger}$, where

$$\gamma_l = \varpi_l \exp(-h\nu_{l1}/kT) . \tag{20}$$

Then,

$$\sum_{l=1}^{\mathcal{N}} Q_{l\kappa}^{\dagger} = \sum_{l=1}^{\mathcal{N}} b_l Q_{l\kappa} . \tag{21}$$

This equation is used to determine any particular b_j, given the ratios b_l/b_j, i.e.,

$$b_j = \left(\sum_{l=1}^{\mathcal{N}} Q_{l\kappa}^{\dagger}\right) \Big/ \left[\sum_{l=1}^{\mathcal{N}} (b_l/b_j) Q_{l\kappa}\right] . \tag{22}$$

To obtain the corresponding number density n_j, we use equation (2), written in the form

$$n_j = n_{\text{total}} \Big/ \left[\sum_{l=1}^{\mathcal{N}} (b_l/b_j)(n_l^*/n_j^*) + (1/b_j)(n_\kappa^*/n_j^*)\right] , \tag{23}$$

while the continuum number density is obtained from

$$n_\kappa = n_{\text{total}} \Big/ \left[1 + \sum_{l=1}^{\mathcal{N}} b_l (n_l^*/n_\kappa^*)\right] . \tag{24}$$

The above equations for b_j and n_j depend on the ratios b_l/b_j, which we determine by solving the statistical-equilibrium equations (4). But before we can discuss how these equations are solved, we need expressions for the bound-bound rate coefficients. These quantities are given by

$$P_{ji} = \mathcal{A}_{ji} + \mathcal{B}_{ji}\bar{J}_{ji} + C_{ji} , \qquad P_{ij} = \mathcal{B}_{ij}\bar{J}_{ji} + C_{ij} \qquad (j > i) . \tag{25}$$

Here $\mathcal{A}_{ji}$, $\mathcal{B}_{ji}$, and $\mathcal{B}_{ij}$ are the Einstein coefficients for spontaneous emission, stimulated emission, and absorption, respectively; C_{ji} and C_{ij} are the collisional de-excitation and excitation rates and are related by

$$C_{ij} = \frac{n_j^*}{n_i^*} C_{ji} . \tag{26}$$

The quantity $\bar{J}_{ji}$ is the total amount of radiation in the ji line defined by

$$\bar{J}_{ji} = \int \varphi_\nu J_\nu d\nu \,, \tag{27}$$

where

$$J_\nu = \frac{1}{4\pi} \int I_\nu d\omega \tag{28}$$

is the mean intensity and φ_ν is the absorption profile normalized so that

$$\int \varphi_\nu d\nu = 1 \,. \tag{29}$$

The $\mathscr{A}$ and $\mathscr{B}$ coefficients are related by

$$\mathscr{A}_{ji} = \left(\frac{2h\nu_{ji}^3}{c^2}\right)\mathscr{B}_{ji} \,, \qquad \varpi_j \mathscr{B}_{ji} = \varpi_i \mathscr{B}_{ij} \,. \tag{30}$$

At large optical depths in any line, the number of absorptions tends to become equal to the number of emissions. The statistical-equilibrium equations then can become poorly conditioned because of dominant radiative terms that nearly cancel out. For this reason we introduce, for the ji transition, the quantity ρ_{ji}, which is proportional to the net radiative rate:

$$n_j(\mathscr{A}_{ji} + \mathscr{B}_{ji}\bar{J}_{ji}) - n_i \mathscr{B}_{ij}\bar{J}_{ji} = n_j \mathscr{A}_{ji}\rho_{ji} \,. \tag{31}$$

Following Thomas (1960), we call ρ_{ji} the net radiative bracket.

If we also define

$$S_{ji} = \frac{2h\nu_{ji}^3/c^2}{(\varpi_j/\varpi_i)(n_i/n_j) - 1} \,, \tag{32}$$

it follows that

$$\rho_{ji} = 1 - \bar{J}_{ji}/S_{ji} \,. \tag{33}$$

Here S_{ji} is the frequency-independent line source function appearing in the radiative-transfer equation for the ji transition when we assume complete redistribution (see § III). At large optical depths, $\bar{J}_{ji}$ may be essentially equal to S_{ji}, while both quantities differ greatly from the Planck function.

Given the above definitions, the statistical equilibrium equation (4) can be written as

$$n_l\left(\sum_{i=1}^{l-1} \mathscr{A}_{li}\rho_{li} + \sum_{m=1(\neq l)}^{\mathscr{N}} Z_{lm}\right) = \sum_{j=l+1}^{\mathscr{N}} n_j \mathscr{A}_{jl}\rho_{jl} + \sum_{m=1(\neq l)}^{\mathscr{N}} n_m Z_{ml} \,, \tag{34}$$

where

$$Z_{ij} = C_{ij} + \mathscr{P}_{ij} \,. \tag{35}$$

Another form of the same equation is

$$b_l\left(\sum_{i=1}^{l-1} \mathscr{A}'_{li}\rho_{li} + \sum_{m=1(\neq l)}^{\mathscr{N}} Z'_{lm}\right) = \sum_{j=l+1}^{\mathscr{N}} b_j \mathscr{A}'_{jl}\rho_{jl} + \sum_{m=1(\neq l)}^{\mathscr{N}} b_m Z'_{ml} \,, \tag{36}$$

where $\mathscr{A}'_{ji} = \gamma_j \mathscr{A}_{ji}$ and $Z'_{ji} = \gamma_j Z_{ji}$ (γ_j was defined by eq. [20]).

Given each $\mathscr{A}'_{ji}\rho_{ji}$, $j > i$, and Z'_{mn}, we use equation (36) for $l = 2, 3, \ldots, \mathscr{N}$ to obtain the set of values b_l/b_1, and from these values, we obtain any b_l/b_j. For example, in the case of a two-level atom,

$$b_2(\mathscr{A}'_{21}\rho_{21} + Z'_{21}) = b_1 Z'_{12} . \tag{37}$$

This way of formulating the statistical-equilibrium equations in terms of net radiative rates utilizes the property that $\rho = 0$ whenever $\bar{J} = S$, which is usually the case at large optical depths. The alternate form of these equations in terms of single bound-bound radiative rates must be used in special cases, as discussed by Avrett (1968).

The statistical-equilibrium equations not only are used to calculate values of b_l/b_j, b_l, and n_l from ρ_{ji} and the various rate coefficients, but also are combined with the radiative-transfer equations to determine each ρ_{ji}. For this purpose, we arrange the multilevel equations in a form similar to that given above for the two-level case.

For the U to L transition of an $\mathscr{N}$-level atom, $\mathscr{N} > 2$, equation (36) for all l except L is written in the form

$$b_U M_{j1} + \sum_{j=2}^{\mathscr{N}-1} b_k M_{ij} = b_L R_i , \qquad i = 1, 2, \ldots, \mathscr{N} , \qquad i \neq L , \tag{38}$$

where M and R are the coefficients resulting from the arrangement of terms. As $j = 2, 3, \ldots, \mathscr{N} - 1$, the corresponding values of k are $1, 2, \ldots, \mathscr{N}$, excluding U and L. The values of b_k, $k \neq U$ or L, are eliminated from this set of equations, so that we obtain a result that resembles equation (37):

$$b_U(\rho_{UL} + \epsilon_1) = b_L \epsilon_2 . \tag{39}$$

General expressions for ϵ_1 and ϵ_2 will be published elsewhere (Avrett and Loeser 1973). We note that ϵ_1 and ϵ_2 depend on ρ_{ji} for transitions $ji \neq UL$, but they do not depend directly on any of the b coefficients.

The line source function S_{UL} can be written as

$$S_{UL} = \frac{2h\nu_{UL}^3/c^2}{(b_L/b_U)\beta^{-1} - 1} , \tag{40}$$

where

$$\beta = \exp(-h\nu_{UL}/kT) . \tag{41}$$

When $b_L/b_U = 1$, S_{UL} becomes the Planck function B_{UL}. If we substitute b_L/b_U from equation (39) into the above expression and use the fact that $\rho_{UL} = 1 - \bar{J}_{UL}/S_{UL}$, we find that

$$S_{UL} = \frac{\bar{J}_{UL} + \epsilon_2(1 - \beta)B_{UL}}{1 + \epsilon_1 - \beta\epsilon_2} \tag{42}$$

or

$$S_{UL} = \frac{\bar{J}_{UL} + \varepsilon_{UL}B^S{}_{UL}}{1 + \varepsilon_{UL}} , \tag{43}$$

where

$$\varepsilon_{UL} = \epsilon_1 - \beta\epsilon_2 \tag{44}$$

and

$$B^S{}_{UL} = \frac{\epsilon_2(1 - \beta)B_{UL}}{\epsilon_1 - \beta\epsilon_2} . \tag{45}$$

Again, ε_{UL} and $B^S{}_{UL}$ depend on ρ_{ji} for transitions $ji \neq UL$ but do not depend directly on any of the b_j coefficients.

We use the radiative-transfer equations to express $\bar{J}_{UL}$ at one depth in the atmosphere in terms of S_{UL} at a discrete number of depths throughout the atmosphere. Then S_{UL} is obtained from the resulting set of equations (43) for each depth. Finally, from equations (33) and (43),

$$\rho_{UL} = \varepsilon_{UL}\left(\frac{B^S{}_{UL}}{S_{UL}} - 1\right) . \tag{46}$$

In this way, we obtain ρ_{ji} for each line transition, and hence the values of b_l and n_l for each atomic level. Iterations are required because the solution for a particular line transition depends on all the others. Moreover, the line solutions both influence and depend on quantities such as the electron density and J_ν in each bound-free continuum. Equations for n_e and J_ν in various continua will be given in later sections.

III. LINE TRANSFER EQUATIONS

Let us consider the specific intensity of radiation I_ν at depth z in a plane-parallel atmosphere and in a direction subtending the angle $\cos^{-1}\mu$ with the outward normal. In general, a number of processes p contribute to the absorption and emission of radiation at the frequency ν, and we write

$$\mu\frac{dI_\nu}{dz} = \sum_p (\kappa_\nu{}^p I_\nu - \eta_\nu{}^p) . \tag{47}$$

The right-hand side can be separated into two parts: the first corresponding to the given line we want to consider, and the second to all continuous processes and any other lines. Therefore,

$$\mu\frac{dI_\nu}{dz} = (\kappa_\nu I_\nu + \eta_\nu) + (\kappa_\nu{}^c I_\nu + \eta_\nu{}^c) . \tag{48}$$

We assume that the line absorption and emission coefficients have the same frequency dependence and that atoms emit radiation with no memory of how they were excited. Then for the UL transition,

$$\kappa_\nu = \frac{h\nu}{4\pi}(n_L\mathscr{B}_{LU} - n_U\mathscr{B}_{UL})\varphi_\nu \tag{49}$$

and

$$\eta_\nu = \frac{h\nu}{4\pi} n_U\mathscr{A}_{UL}\varphi_\nu . \tag{50}$$

The line source function $S = \eta_\nu/\kappa_\nu$ is then independent of frequency, and the scattering of line radiation is said to be completely noncoherent. This assumption of frequency independence, also called complete redistribution, is regarded as a reasonable approximation for the source-function calculation in most astrophysical problems (see Thomas 1957; Jefferies and White 1960; Avrett and Hummer 1965; Hummer 1969).

From equations (30) for the Einstein coefficients, the ratio η_ν/κ_ν reduces to the expression for S given by equation (32). The profile φ_ν in the above equations is the same that appears in equation (27) for $\bar{J}$. We will specify φ_ν as a function of frequency and depth for each line in § IX.

The transfer equation can be written as

$$\mu \frac{dI_\nu}{dz} = \kappa_\nu(I_\nu - S) + \kappa_\nu^c(I_\nu - S_\nu^c)\,, \tag{51}$$

where

$$S_\nu^c = \eta_\nu^c/\kappa_\nu^c\,. \tag{52}$$

We introduce the monochromatic optical depth τ_ν so that

$$d\tau_\nu = (\kappa_\nu + \kappa_\nu^c)dz\,, \tag{53}$$

and define $\phi_\nu = \kappa_\nu/\kappa_{\nu_0}$ and $r_\nu = \kappa_\nu^c/\kappa_{\nu_0}$, where ν_0 is the line-center frequency. The transfer equation then becomes

$$\mu dI_\nu/d\tau_\nu = I_\nu - S_\nu\,, \tag{54}$$

where

$$S_\nu = \frac{\phi_\nu}{\phi_\nu + r_\nu} S + \frac{r_\nu}{\phi_\nu + r_\nu} S_\nu^c\,; \tag{55}$$

and for a semi-infinite atmosphere with no incident radiation,

$$J_\nu(\tau_\nu) = \frac{1}{2}\int_0^\infty E_1(|t_\nu - \tau_\nu|)S_\nu(t_\nu)dt_\nu\,, \tag{56}$$

where E_1 is the first exponential integral function.

Let us now write this expression for J_ν in discrete form. We let the subscripts i and j refer to any of N prescribed depths in the atmosphere, and we let k refer to a given frequency. Given a functional representation of S_ν in terms of unknown discrete values, equation (56) can be expressed in the form

$$J_{ik} = \sum_{j=1}^{N} W_{ijk}^{(\Lambda)} S_{jk} \tag{57}$$

(see Avrett and Loeser 1969 for details). Equation (27) for $\bar{J}$ can be written as

$$\bar{J}_i = \sum_{k=1}^{K} \gamma_{ik} J_{ik}\,, \tag{58}$$

where the coefficients γ_{ik} are normalized such that

$$\sum_{k=1}^{K} \gamma_{ik} = 1\,. \tag{59}$$

Then,

$$\bar{J}_i = \sum_{j=1}^{N}\sum_{k=1}^{K} \gamma_{ik} W_{ijk}^{(\Lambda)} \left[\left(1 - \frac{r_{jk}}{\phi_{jk} + r_{jk}}\right) S_j + \frac{r_{jk}}{\phi_{jk} + r_{jk}} S_{jk}^c\right]. \tag{60}$$

We combine this expression with equation (43), i.e.,

$$S_i = \frac{\bar{J}_i + \varepsilon_i B_i^S}{1 + \varepsilon_i} , \tag{61}$$

and solve the resulting set of linear equations for the values S_i, $i = 1, 2, \ldots, N$.

There are several ways of rearranging terms on the right-hand side of equation (60), and of combining equations (60) and (61); but all are equivalent provided that the coefficients γ_{ik} are normalized as indicated and that the weighting coefficients $W_{ijk}^{(\Lambda)}$ are determined with proper care. The various ways of writing the equations are reviewed by Avrett (1971), and the $W_{ijk}^{(\Lambda)}$ calculation is discussed in detail by Avrett and Loeser (1969). This method for the source-function determination is equivalent to that proposed by Athay and Skumanich (1967).

IV. LYMAN-CONTINUUM EQUATIONS

In the foregoing section, we combined the equations of radiative transfer and statistical equilibrium to obtain a set of simultaneous equations for the line source function at each depth. Here, we derive the analogous equations for the bound-free case—in particular, the solar Lyman continuum.

The statistical-equilibrium equation for level l is given by equation (1). Such equations for $l = 2, 3, \ldots, \mathcal{N}$ can be used to eliminate $n_2, n_3, \ldots$ from the continuum equation

$$n_\kappa \left(P_{\kappa 1} + \sum_{j=2}^{\mathcal{N}} P_{\kappa j} \right) = n_1 P_{1\kappa} + \sum_{j=2}^{\mathcal{N}} n_j P_{j\kappa} . \tag{62}$$

We can write the result as

$$n_\kappa (P_{\kappa 1} + L) = n_1 (P_{1\kappa} + U) . \tag{63}$$

From equations (13) and (16), it follows that

$$P_{1\kappa}{}^\dagger + \frac{n_\kappa{}^*}{n_1{}^*} L = b_1 (P_{1\kappa} + U) . \tag{64}$$

Then,

$$\frac{1}{b_1} = \frac{R_{1\kappa} + C_{1\kappa} + U}{R_{1\kappa}{}^\dagger + C_{1\kappa} + (n_\kappa{}^*/n_1{}^*) L} . \tag{65}$$

Since stimulated emission is completely negligible throughout the solar Lyman continuum, we replace $R_{1\kappa}{}^\dagger$ by

$$R_{1\kappa}{}^* = 4\pi \int_{\nu_{\kappa 1}}^{\infty} \frac{1}{h\nu} \alpha_1(\nu) B'_\nu d\nu , \tag{66}$$

where

$$B'_\nu = \frac{2h\nu^3}{c^2} e^{-h\nu/kT} . \tag{67}$$

Let

$$J_L = \frac{R_{1\kappa}}{R_{1\kappa}^*}, \tag{68}$$

$$\epsilon_L = \frac{1}{R_{1\kappa}^*}\left(C_{1\kappa} + \frac{n_\kappa^*}{n_1^*} L\right), \tag{69}$$

and

$$\eta = \frac{1}{R_{1\kappa}^*}(C_{1\kappa} + U). \tag{70}$$

Equation (65) then becomes

$$\frac{1}{b_1} = \frac{J_L + \eta}{1 + \epsilon_L}. \tag{71}$$

The defining expression for J_L can also be written as

$$J_L = \left(\int_{\nu_{\kappa 1}}^{\infty} \alpha' J_\nu d\nu\right) \Big/ \left(\int_{\nu_{\kappa 1}}^{\infty} \alpha' B'_\nu d\nu\right), \tag{72}$$

where $\alpha'(\nu) = \alpha_1(\nu)/\nu$. The above equation for $1/b_1$ in terms of J_L is analogous to equation (61) for S in terms of $\bar{J}$.

The transfer equation for the Lyman continuum is given by

$$\mu \frac{dI_\nu}{dz} = n_1 \alpha_1(\nu)\left(I_\nu - \frac{1}{b_1} B'_\nu\right), \tag{73}$$

where, again, stimulated emission is ignored. In the present calculations we also ignore absorption and emission in the Lyman continuum due to atoms other than hydrogen.

As in the case of the line transfer equations, we can determine the weighting coefficients W such that the mean intensity at depth i is given by

$$J_{ik} = \sum_{j=1}^{N} W_{ijk}^{(\Lambda)} S_{jk}, \tag{74}$$

where in the present case

$$S_{jk} = \frac{1}{b_{1j}} B'_{jk}. \tag{75}$$

(Here, b_{1j} refers to b_1 at depth j.) We substitute these equations into equation (72) and introduce the frequency weights a_k so that

$$J_{Li} = \left(\sum_{j=1}^{N} \frac{1}{b_{1j}} \sum_{k=1}^{K} a_k W_{ijk}^{(\Lambda)} B'_{jk}\right) \Big/ \left(\sum_{k=1}^{K} a_k B'_{ik}\right). \tag{76}$$

This expression is combined with

$$\frac{1}{b_{1i}} = \frac{J_{Li} + \eta_i}{1 + \epsilon_{Li}}, \qquad i = 1, 2, \ldots, N, \tag{77}$$

and we solve the resulting set of equations for $1/b_1$ at each depth. Here, ϵ_L and η are

considered known. Given $1/b_1$, we have J_L from equation (77). Then from the definition of J_L, the photoionization rate is given by

$$R_{1\kappa} = J_L R_{1\kappa}^* \,. \tag{78}$$

We obtain $R_{i\kappa}$ in this way only in the case of the hydrogen Lyman continuum. Other photoionization rates are determined iteratively; i.e., given the level populations, we find the continuum source functions and integrate to determine J_ν, then $R_{i\kappa}$, then new level populations, etc. Here such a procedure would reduce to the solution of equations (76) and (77) by successive iteration, and the solution would converge slowly as a consequence of the facts that (1) $\epsilon_L \ll 1$ and (2) absorption and emission by other processes are negligible. These conditions do not apply to the other bound-free continua considered here, and in those cases the iterative determinations of the photoionization rates converge rapidly.

We note that b_1 is given by equation (22) as well as by equation (77). In equation (22), b_1 depends on the bound-free rates, on the b_l/b_j ratios, and, in equation (77), on the bound-free and bound-bound rates. Given the same bound-free rates and given consistency between the b_l/b_j ratios and the bound-bound rates, both equations imply the same numerical values for b_1.

V. THE ELECTRON NUMBER DENSITY

In the preceding section, we described the calculation of b_1, the hydrogen ground-level departure coefficient. Now we show how n_e is determined, given that the electron number density both influences and depends on the ionization of hydrogen and that it also depends on the ionization of other atoms.

From the assumption of charge neutrality, the electron density is given by

$$n_e = n_p + n_{\rm H} \sum_\xi A_\xi \eta_\xi \,, \tag{79}$$

where n_p is the proton number density, $n_{\rm H}$ is the total hydrogen number density (neutral atoms plus protons), A_ξ is the abundance relative to hydrogen of any other constituent, and η_ξ is the corresponding degree of ionization.

We let

$$\psi(T) = \left(\frac{h^2}{2\pi m k T}\right)^{3/2} \exp\left(\chi_{\rm H}/kT\right) , \tag{80}$$

so that

$$n_1 = n_e n_p b_1 \psi(T) \,. \tag{81}$$

We combine equations (79) and (81) with

$$n_1\left(1 + \sum_{l=2}^{\mathcal{N}} \frac{n_l}{n_1}\right) + n_p = n_{\rm H} \tag{82}$$

to eliminate n_1 and n_p. The result is a quadratic equation for n_e, which has the solution

$$n_e = \frac{[(1 + Z d n_{\rm H})^2 + 4 d n_{\rm H}]^{1/2} - (1 - Z d n_{\rm H})}{2d} \,, \tag{83}$$

where

$$Z = \sum_\xi A_\xi \eta_\xi \tag{84}$$

and

$$d = b_1\psi(T)\left(1 + \sum_{l=2}^{\mathcal{N}} \frac{n_l}{n_1}\right) . \tag{85}$$

In the present calculations, we determine Z from the first ionization equilibria of the atoms listed in table 1. We calculate in detail the ionization of carbon and silicon, but use the Saha equation to find the degree of ionization in each of the other cases, i.e.,

$$\eta_\xi = \frac{1}{1 + n_e\Psi_\xi(T)} , \tag{86}$$

where

$$\Psi_\xi(T) = \left(\frac{h^2}{2\pi mkT}\right)^{3/2}\left(\frac{U_{\rm I}}{2U_{\rm II}}\right)_\xi \exp\left(\chi_\xi/kT\right) . \tag{87}$$

Since Z depends on n_e, we solve equations (83) and (86) by successive iterations. (Only a few are required.)

Our adopted values of abundance A, ionization potential χ, and partition functions $U_{\rm I}$ and $U_{\rm II}$ (assumed constant) are given in table 1. The abundance values in this table are from the review by Withbroe (1971). Helium contributes electrons only in the chromosphere-corona transition region, where $T > 10{,}000°$ K. The other atoms listed in the table contribute electrons only in the photosphere and low chromosphere, where $T < 6000°$ K. Otherwise, $n_e = n_p$.

The equations in this section show that n_e depends primarily on the functions b_1, T, and $n_{\rm H}$. The term $\sum n_l/n_1$, $l > 1$, is usually very small compared to unity, but is evaluated in any case from the ratios b_l/b_1.

TABLE 1

DATA USED IN THE ELECTRON-DENSITY CALCULATION

Element	A	$\log A + 12$	χ (eV)	$U_{\rm I}$	$U_{\rm II}$
He	1.00(−1)	11.00	24.58	1.00	2.00
C	5.37(−4)	8.73	11.26	9.28	5.94
N	1.14(−4)	8.06	14.53	4.07	8.91
O	6.76(−4)	8.83	13.61	8.70	3.98
Ne	3.54(−5)	7.55	21.55	1.00	5.37
Na	2.81(−6)	6.45	5.14	2.02	1.00
Mg	4.46(−5)	7.65	7.64	1.01	2.01
Al	2.81(−6)	6.45	5.98	5.83	1.03
Si	4.46(−5)	7.65	8.15	9.26	5.82
P	2.81(−7)	5.45	10.48	4.46	8.12
S	1.62(−5)	7.21	10.35	8.12	4.16
Ar	5.62(−6)	6.75	15.75	1.00	4.89
K	5.62(−7)	5.75	4.33	2.18	1.00
Ca	2.51(−6)	6.40	6.11	1.03	2.29
Cr	7.07(−7)	5.85	6.76	10.3	7.24
Mn	3.54(−7)	5.55	7.43	6.45	7.76
Fe	2.50(−5)	7.40	7.83	24.5	39.2
Co	2.23(−7)	5.35	7.86	31.6	27.5
Ni	3.38(−6)	6.53	7.63	28.8	10.0

VI. HYDROSTATIC EQUILIBRIUM

Here we show how n_H is determined as a function of depth, given n_e, b_1, T, and the function v_t. We assume that the atmosphere is static, so that the pressure p and density ρ are related by

$$dp/dz = g\rho\,, \tag{88}$$

where g is the gravitational constant, and z represents geometrical depth, measured inward. The gas density can be written as

$$\rho = m_H(1 + 4Y)n_H\,, \tag{89}$$

where m_H is the hydrogen atomic mass and $Y = A_{He} = n_{He}/n_H$. The gas pressure is

$$p_g = [n_H(1 + Y) + n_e]kT\,, \tag{90}$$

and we assume a turbulent-pressure contribution to the total pressure such that

$$p = p_g + \tfrac{1}{2}\rho v_t^2\,. \tag{91}$$

The turbulent-velocity parameter v_t is a specified function of depth. Equation (79) for the electron density can be written in the form

$$n_e = n_H(R + Z)\,, \tag{92}$$

where $R = n_p/n_H$.

We define a reciprocal scale height according to

$$f = \frac{gm_H(1 + 4Y)}{(1 + R + Y + Z)kT + (1/2)m_H(1 + 4Y)v_t^2}\,. \tag{93}$$

The hydrostatic equilibrium equation (88) then becomes

$$dp/dz = fp\,, \tag{94}$$

so that

$$p(z) = p(z_1)\exp\left[\int_{z_1}^{z} f(x)dx\right]. \tag{95}$$

From $p(z)$, we can finally determine

$$n_H(z) = \frac{f(z)p(z)}{gm_H(1 + 4Y)}\,. \tag{96}$$

The pressure $p(z_1)$ at the outermost depth is found automatically in the following way. A given $p(z_1)$ allows us to determine $p(z)$, the various number densities, and the optical depth at 5000 Å as functions of z. By successive approximations, we adjust $p(z_1)$ such that $\tau_{5000} = 1$ at $z = 0$ (z_1 is then negative). We define height in kilometers by $h = -10^{-5}z$ (z in cm). The assumed T and v_t are thus specified against height measured above the level at which $\tau_{5000} = 1$.

The functions of height appearing in equation (93) for the reciprocal scale height are the following: T and v_t, which are assumed given; Z, which is determined along with n_e by the equations in § V; and finally the ratio $R = n_p/n_H$. From equation (24), we can write

$$R = \frac{1}{1 + dn_e}\,, \tag{97}$$

where d is given by equation (85).

VII. CONTINUUM DATA

We need to calculate values of the continuum opacity κ^c and the continuum source function S^c, at various wavelengths, because (1) they are required for the solution of each line transfer equation (see § III), (2) they are necessary for calculating the mean intensity J_ν, which, in turn, enters the equation for each photoionization rate (see eq. [8] and § IX), and (3) they are required for calculating the emergent intensities, as described in § VIII.

In the present section, we first show how S^c and J_ν are computed, given the various absorption and scattering opacities and constituent source functions. Then we list and specify the individual opacity and source-function contributions.

Let σ be the total scattering opacity and κ^{ab} the opacity due to the sum of all other absorbers. The scattering source function is assumed to be the mean intensity J (frequency subscripts are omitted here), and we introduce an absorption source function given by

$$S^{ab} = \frac{1}{\kappa^{ab}} \sum_m \kappa_m S_m{}^c , \tag{98}$$

where

$$\kappa^{ab} = \sum_m \kappa_m \tag{99}$$

and where $S_m{}^c$ is the constituent source function corresponding to the individual opacity κ_m. The transfer equation for the particular continuum wavelength is then

$$\mu \frac{dI}{dz} = \sigma(I - J) + \kappa^{ab}(I - S^{ab}) , \tag{100}$$

which becomes

$$\mu dI/d\tau_c = I - S^c \tag{101}$$

if we define

$$d\tau_c = (\sigma + \kappa^{ab})dz \tag{102}$$

and

$$S^c = (1 - \alpha)J + \alpha S^{ab} , \tag{103}$$

where

$$\alpha = \frac{\kappa^{ab}}{\sigma + \kappa^{ab}} . \tag{104}$$

From equation (101) we can express J in terms of the values of S^c as

$$J_i = \sum_{j=1}^{N} W_{ij}{}^{(\Lambda)} S_j{}^c . \tag{105}$$

The N values of S^c are determined from the N simultaneous equations

$$S_i{}^c - (1 - \alpha_i) \sum_{j=1}^{N} W_{ij}{}^{(\Lambda)} S_j{}^c = \alpha_i S_i{}^{ab} . \tag{106}$$

The mean intensity then follows from equation (103) or (105).

Here, τ_c, S^c, and J depend on the scattering and absorption coefficients σ and κ^{ab} and on the absorption source function S^{ab}. In the determination of σ, we include the electron scattering contribution $6.653 \times 10^{-25} n_e$, together with Rayleigh scattering as given by Gravila (1967). We treat the natural damping opacity in the Lα line wings as Rayleigh scattering, except for a small proportion that we associate with non-coherent scattering. Details of these estimates will be given in a subsequent paper (see also § XI).

The remaining opacities included in equation (99) for κ^{ab} are the following:

a) H and H^- free-free absorption for which $S_c^m = B$, the Planck function.

b) Bound-free helium, aluminum, magnesium, iron, calcium, and sodium (all neutral) for which at present we assume, for simplicity, that $S_c^m = B$.

c) Bound-free H, C I, and Si I for which we determine κ^m and S_c^m from explicitly calculated number densities. For hydrogen, we use the photoionization cross-sections given by Menzel and Pekeris (1935) with frequency-dependent Gaunt factors given by Karsas and Latter (1961). The numerical data we use for carbon, silicon, and the other opacities listed above will be given in subsequent papers.

d) Bound-free H^-, the equations for which are as follows. The departure coefficient $b_{H^-} = n_{H^-}/n^*_{H^-}$, which occurs in the H^- bound-free absorption coefficient and in the constituent source function

$$S^c_{H^-} = \frac{2h\nu^3/c^2}{b_{H^-} e^{h\nu/kT} - 1}, \tag{107}$$

is given by

$$b_{H^-} = \frac{R^\dagger + r}{R + r}, \tag{108}$$

where R is the photodetachment rate

$$R = 4\pi \int_{\nu_0}^{\infty} \alpha_\nu J_\nu \frac{d\nu}{h\nu} \tag{109}$$

and

$$R^\dagger = 4\pi \int_{\nu_0}^{\infty} \alpha_\nu e^{-h\nu/kT} \left(\frac{2h\nu^3}{c^2} + J_\nu \right) \frac{d\nu}{h\nu}. \tag{110}$$

The quantity r is given by

$$r = r_e + \frac{r_H}{1 + (r_H n^*_{H^-}/r_{3H} n_H)}, \tag{111}$$

where r_H and r_e are the associative detachment and electron collisional detachment rates per H^- ion, respectively, and r_{3H} is the rate per H atom for the three-body collision process $3H \rightarrow H_2 + H$. According to Browne and Dalgarno (1969),

$$r_H = 2.10 \times 10^{-9} n_H. \tag{112}$$

Also, as discussed by Gebbie and Thomas (1970),

$$r_e = 2.0 \times 10^{-9} n_e \theta^{-3/2} \tag{113}$$

and

$$r_{3H} = 10^{-32} n_H^2 \theta , \tag{114}$$

where $\theta = 5040/T$. Finally,

$$n^*_{H^-} = 2.89 \times 10^{-22} n_H n_e \theta^{3/2} e^{1.736\theta} . \tag{115}$$

VIII. EMERGENT INTENSITIES

We have given equations in the previous section and in § III for the monochromatic optical depth τ_ν and the source function S_ν at any frequency in the continuum or within any line. The emergent continuum intensities throughout the spectrum and the intensity profiles of each line can then be computed by the standard formula

$$I_\nu(\mu) = \frac{1}{\mu} \int_0^\infty S_\nu(\tau_\nu) \exp(-\tau_\nu/\mu) d\tau_\nu , \tag{116}$$

where μ is the cosine of the angle between the direction of radiation and the outward normal.

We determine a monochromatic brightness temperature T_B from any given I_ν by the equation

$$I_\nu = \frac{2h\nu^3/c^2}{\exp(h\nu/kT_B) - 1} . \tag{117}$$

Our computed microwave spectrum (§ XI) is given in terms of T_B at $\mu = 1$.

IX. PRESCRIBED DATA

a) The Atomic Model

We specify the bound energy levels of a given atom or ion and the continuum level corresponding to the next higher stage of ionization. Thus, we give the frequency measured from the ground level to each bound level and to the continuum edge, the statistical weight ϖ_l for each level, and the partition function U for the continuum.

The electron-atom collisional ionization parameter $\Omega_l(T)$ is given as a function of temperature for each level l such that the collisional ionization rate (per atom in level l) is

$$C_{l\kappa} = n_e \Omega_l(T) \exp(-h\nu_{\kappa l}/kT) . \tag{118}$$

The collisional recombination rate (per ionized atom) is then given by

$$C_{\kappa l} = n_e^2 \Omega_l(T) \frac{\varpi_l}{2U_\kappa} \left(\frac{h^2}{2\pi mkT}\right)^{3/2} \tag{119}$$

according to equations (12) and (11). Usually, $\Omega_l(T)$ is a slowly varying function of temperature.

We specify the photoionization cross-section $\alpha_l(\nu)$ for level l at the limiting continuum frequency $\nu_{\kappa l}$ and at several frequencies in the range $\nu > \nu_{\kappa l}$. The mean intensity J_ν is determined as a function of depth for each ν by the procedure discussed in § VII. The photoionization rate is then determined by

$$R_{l\kappa} = 4\pi \int_{\nu_{\kappa l}}^{\nu_l^{\max}} \frac{1}{h\nu} \alpha_l(\nu) J_\nu d\nu + r_{l\kappa} , \tag{120}$$

where the integral from $\nu_{\kappa l}$ to $\nu_l^{\max}$ is evaluated numerically and $r_{l\kappa}$ is an approximation to the integral from $\nu_l^{\max}$ to ∞. To evaluate $r_{l\kappa}$, we assume that $\alpha_l(\nu)$ varies as $\alpha_l(\nu_l^{\max})(\nu_l^{\max}/\nu)^3$ in the range $\nu \geq \nu_l^{\max}$ and that J_ν varies as

$$J_\nu = (2h\nu^3/c^2) \exp(-h\nu/kT_{rl}^m),$$

where T_{rl}^m is determined from J_ν by this equation with $\nu = \nu_l^m$. It then follows that

$$r_{l\kappa} = \frac{8\pi}{c^2}(\nu_l^{\max})^3 \alpha_l(\nu_l^{\max}) E_1\left(\frac{h\nu_l^{\max}}{kT_{rl}^m}\right). \tag{121}$$

The radiative recombination rate is given by equation (9). As explained at the end of § IV, we use a different procedure to obtain $R_{l\kappa}$ for the $l = 1$ Lyman continuum of hydrogen.

For the bound-bound transitions, we need radiative rates, collisional rates, and line-broadening parameters. We specify Einstein $\mathscr{A}$ coefficients for each radiative transition and determine radiative rates by the equations of § II, given the values of $\bar{J}$ or ρ that we calculate along with each line source function.

In analogy with the above expression for the collisional ionization rate, we obtain the collisional excitation rate for the UL transition, $U > L$, according to

$$C_{LU} = n_e \Omega_{UL}(T) \exp(-h\nu_{UL}/kT), \tag{122}$$

where $\Omega_{UL}(T)$ is a given function of temperature, and a slowly varying one in most cases. The collisional deexcitation rate is then

$$C_{UL} = n_e \Omega_{UL}(T) \varpi_L/\varpi_U. \tag{123}$$

The Doppler width of each line is generated by the expression

$$\Delta\lambda_D\,(\text{Å}) = 0.091 \frac{\lambda\,(\text{Å})}{3000}\left[\frac{1}{M}\frac{T}{5000} + \left(\frac{V}{9.1}\right)^2\right]^{1/2}, \tag{124}$$

where M is the atomic mass relative to hydrogen. The velocity parameter V is in units of km s^{-1} and is discussed in § XI.

Values of the damping parameter in angstrom units for each line are obtained by the formula

$$\delta\,(\text{Å}) = C_{\text{rad}} + C_{\text{vdW}}\left(\frac{n_{\text{H I}}}{10^{16}}\right)\left(\frac{T}{5000}\right)^{0.3} + C_{\text{Stk}}\left(\frac{n_e}{10^{12}}\right)^p, \tag{125}$$

where $n_{\text{H I}}$ is the neutral-hydrogen number density; the constants C_{rad}, C_{vdW}, and C_{Stk} specify the radiative, van der Waals, and Stark half-widths, respectively; and p depends on whether the Stark effect for the particular atom is linear or quadratic.

The normalized line absorption coefficient in equations (27), (49), and (50) is assumed given by the Voigt function

$$\varphi_\nu = \frac{a}{\Delta\nu_D \pi^{3/2}} \int_{-\infty}^{+\infty} \frac{e^{-x^2} dx}{a^2 + [x - (\nu - \nu_0)/\Delta\nu_D]^2}, \tag{126}$$

where $a = \delta\,(\text{Å})/\Delta\lambda_D\,(\text{Å})$, and where $\Delta\nu_D$ is related to $\Delta\lambda_D$ by $\Delta\nu_D/\nu = \Delta\lambda_D/\lambda$. In the case of zero damping or pure Doppler broadening, the above expression reduces to

$$\varphi_\nu = \frac{1}{\Delta\nu_D\sqrt{\pi}} \exp\{-[(\nu - \nu_0)/\Delta\nu_D]^2\}. \tag{127}$$

Note that φ_ν depends on depth as well as on frequency because of the depth dependence of T, V, $n_{\mathrm{H\,I}}$, and n_e.

b) The Atmospheric Model

We specify a set of geometrical height values h_i, $i = 1, 2, \ldots, N$, and corresponding values of temperature T_i and velocity V_i. The pressure scale is adjusted so that $\tau_{5000} = 1$ at the point where $h = 0$ (see § VI). As explained in § VI, we use V both as a microturbulent velocity in line broadening and as a turbulent pressure velocity. The equations given in § II through § VII are used to determine all other functions of depth; these include pressure, density, electron number density, atomic populations, departure coefficients, source functions, opacities, optical depths, rate coefficients, net rates, and the mean intensity and flux of radiation at each depth and given wavelength.

X. THE SEQUENCE OF CALCULATIONS

By use of the techniques and equations described in the preceding sections, PANDORA calculates a synthetic spectrum as follows, given T and V as functions of geometrical depth and given the various atomic parameters.

a) The input data consist of the quantities discussed in § IX and the starting values of a number of other depth-dependent functions—namely, the electron density; the total hydrogen density; bound-level and ionized number densities of hydrogen, carbon, and silicon; values of the net radiative bracket for all radiative transitions of the particular atom; and, in the case of hydrogen, the Lyman-continuum photoionization rate. LTE equations are used to generate these starting values unless non-LTE values are available from a previous PANDORA run.

b) The continuum opacities, continuum source functions, and mean intensities are computed at various wavelengths, as described in § VII. The H^- departure coefficient is obtained by means of equation (108). Photoionization rates are determined from several values of J_ν in each of the ionization continua.

c) Given the bound-free radiative rates, the collisional rates, and values of ρ_{UL} for each transition, we calculate b_l and n_l from equations (36), (22), and (23). The monochromatic optical depths for each line are then determined by equations (49) and (53) and by the equations for the profile function φ_ν given in § IX.

d) The coupling parameters ϵ_1 and ϵ_2 are calculated for each line according to equations (38) and (39). We find each line source function by the combined equations (61) and (60). Then a new ρ is determined by equation (46). In this way, we establish an improved set of the net radiative brackets ρ_{UL} for each line. This step is usually repeated at least once before we proceed further.

e) In the hydrogen case, we find the Lyman-continuum coupling parameters ϵ_L and η and then solve for $1/b_1$ and $R_{1\kappa}$ as described in § IV. We recompute the electron number density by the equations given in § V and solve the hydrostatic-equilibrium equations (§ VI) to establish a new total hydrogen density distribution. In cases other than hydrogen, n_e is changed according to the ionizing contribution of the particular atom, but we do not solve the Lyman-continuum or hydrostatic-equilibrium equations.

f) The improved ρ_{UL} set and the other recomputed functions are used to calculate new values of the bound-level and ionized number densities of the particular atom (hydrogen, carbon, or silicon).

g) These number densities and the other recalculated functions replace those in step *a*, and another overall iteration (steps *b*–*f*) is carried out. The hydrogen calculations converge in about eight overall iterations, while the carbon and silicon calculations each require about four such iterations. The hydrogen solution is essentially independent of the carbon and silicon solutions, while the latter two depend on the former and on each other. The hydrogen, carbon, and silicon calculations are carried

out in the following sequence: hydrogen, silicon, carbon, silicon, and carbon; each calculation uses results established earlier in the sequence.

XI. SUMMARY OF THE SOLAR MODEL CALCULATIONS

We have determined an empirical temperature distribution for the solar photosphere, chromosphere, and chromosphere-corona transition region such that the predicted continuous intensity spectrum agrees with observed continuous intensities from quiet regions near the center of the solar disk for wavelengths extending from 505 Å in the extreme ultraviolet to 1.5 cm in the extreme-infrared. We also obtain general agreement between predicted and observed profiles of the Lα, Lβ, Hα, Hβ, and Pα lines. In addition, some features of the model are based on profiles of the Ca II H and K lines and infrared triplet lines.

We solve the hydrostatic-equilibrium equation and the radiative-transfer and statistical-equilibrium equations for a six-level hydrogen atom and for eight-level C I and Si I atoms. All radiative transitions are treated explicitly. The present calculation of the continuous absorption and emission throughout the spectrum, and the calculation of n_e, take into account the non-LTE contribution of H^- in addition to H, C I, and Si I and the LTE contributions of helium, aluminum, magnesium, iron, calcium, sodium, and the other elements listed in table 1. The details of these calculations will appear in subsequent papers.

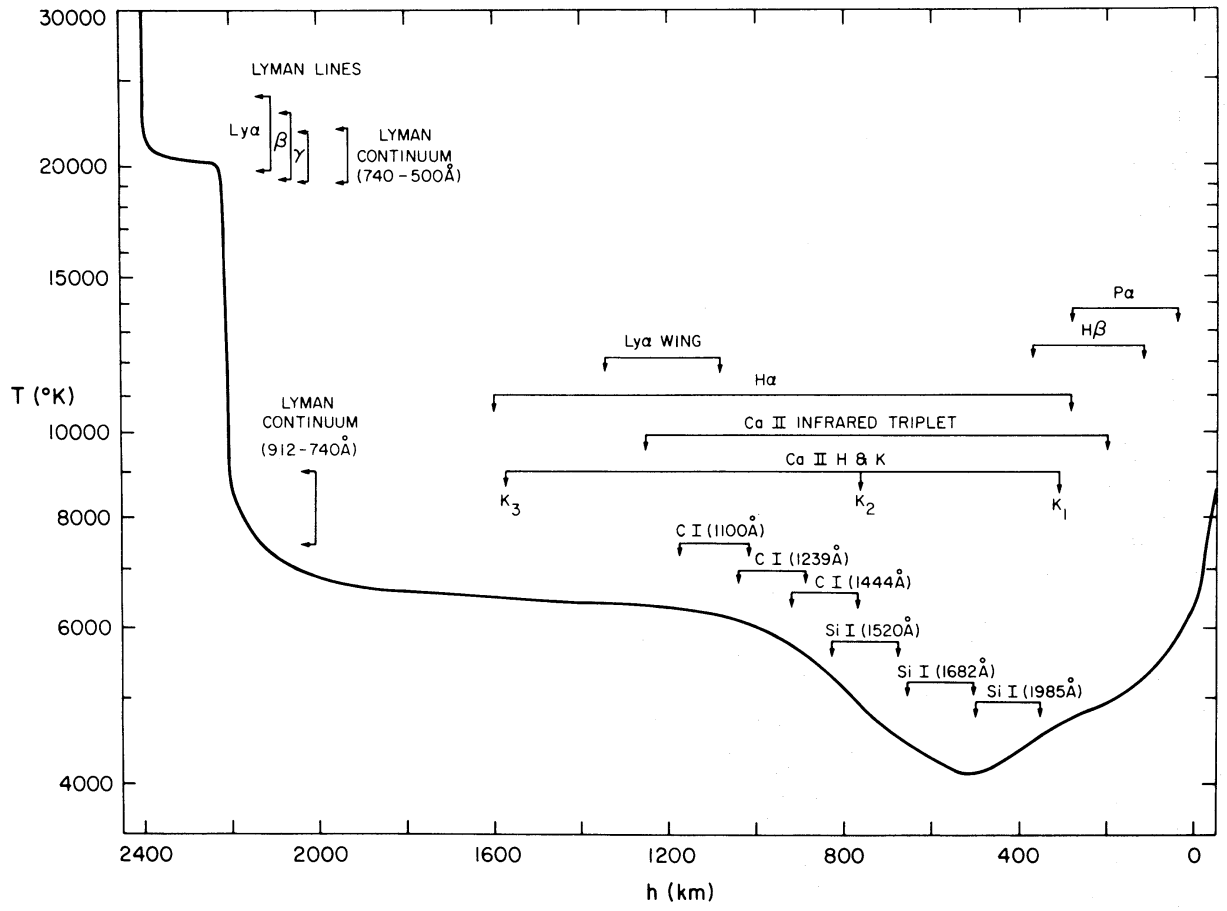

FIG. 1.—Our adopted temperature-height distribution for the photosphere (on the right), temperature-minimum, chromosphere, and chromosphere-corona transition zone. Also indicated are the regions of formation of the various lines and continua we have studied.

In figure 1, we show the temperature as a function of height. Height is given in kilometers measured above a zero point where $\tau_{5000} = 1$. Also indicated in the figure are the regions of formation of line and continuum intensities on which we base the model. In the photosphere, our temperature distribution is the same as that of the Harvard-Smithsonian Reference Atmosphere (Gingerich *et al.* 1971), but our temperature values are lower in the region between 400 and 500 km. We have adopted a temperature-minimum value of 4100° K located at 520 km. At about 1000 km, where the three lowest C I continua are formed, the temperature has risen to 6000° K. In the region between 1000 and 2200 km, the continuous spectrum provides little direct information about the temperature structure, and the values we have adopted are somewhat arbitrary.

The sharp temperature rise from about 8500° K at 2200 km to much higher temperatures in the chromosphere-corona transition region is interrupted by a plateau at approximately 20,000° K having a width of about 250 km. This plateau has been introduced in order that the optical thickness in the Lyman lines (particularly Lβ) is sufficiently great to produce central reversals, as observed by Tousey (1963). Chipman (1971) also found evidence, based on the center-to-limb behavior of the C II resonance lines, for a plateau in this region.

Such a high-temperature plateau increases the calculated intensities in the short-wavelength tail of the Lyman continuum (740–500 Å) and leads to better agreement with observations (see Vernazza and Noyes 1972). The plateau, together with lower portions of the transition region, also contributes to the intensity in the leading part of the Lyman continuum from 912 to 740 Å. To balance this contribution, we have temperatures in the chromosphere just below the transition region that are lower than the corresponding temperatures from chromospheric models that do not include a transition region (Noyes and Kalkofen 1971; Gingerich *et al.* 1971). We will give detailed comparisons with other models in a subsequent paper.

In table 2, we give an abbreviated list of the values of temperature and velocity used to obtain the synthetic spectrum shown in this paper; the velocity distribution is shown later in this section. A more complete tabulation of the model will appear in another paper of this series.

Our temperature determination may be in error owing to observational uncertainties and to oversimplifications and shortcomings in our theoretical approach. Observational uncertainties lead to temperature errors of the order $\pm 100°$ K near the tem-

TABLE 2

TEMPERATURE AND VELOCITY VALUES FOR THE PRESENT MODEL*

h	T	V	h	T	V
−75.....	9300	1.0	1000.....	6100	2.5
−50.....	8500	1.0	1200.....	6300	3.5
−25.....	7100	1.0	1400.....	6400	5.1
0.....	6400	1.0	1600.....	6500	6.2
50.....	5750	1.0	1800.....	6600	7.6
100.....	5400	1.0	2000.....	6800	9.0
200.....	4900	1.0	2100.....	7300	9.7
300.....	4600	1.0	2200.....	8400	10.3
400.....	4400	1.0	2220.....	15000	10.5
500.....	4100	1.0	2230.....	20000	10.6
600.....	4300	1.1	2300.....	20300	11.0
700.....	4600	1.2	2390.....	21000	11.8
800.....	5000	1.4	2400.....	25000	11.9
900.....	5600	1.9	2410.....	35000	12.0

* We are continuing to refine the model; updated tables that lead to better agreement with available data will appear in subsequent papers of this series.

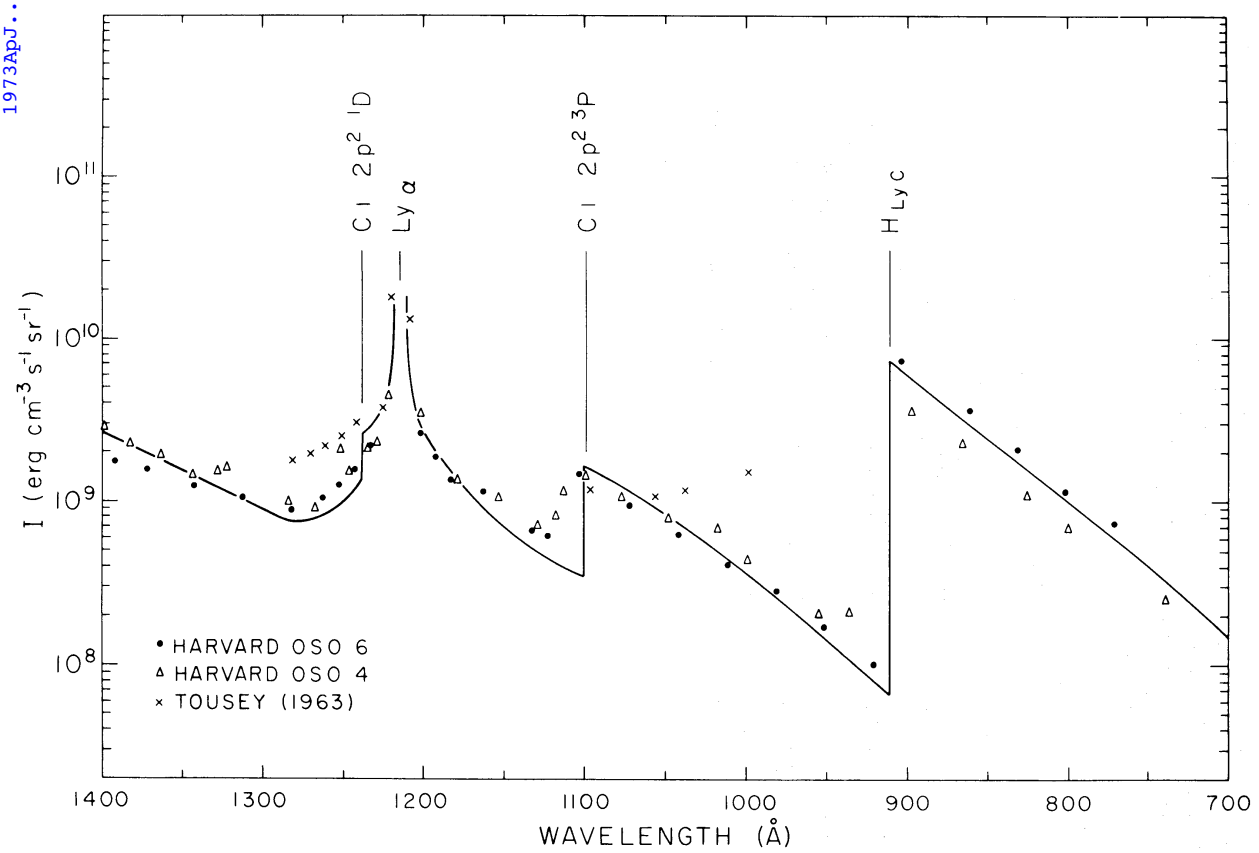

FIG. 2.—Predicted and observed intensities for quiet regions near disk center in the wavelength region 700–1400 Å.

perature minimum and ±200° K in the upper chromosphere, while the 20,000° K temperature plateau has an uncertainty of as much as ±2000° K. Our theoretical approach is based on an effort to understand the solar spectrum as fully as possible in terms of a static atmosphere having properties that vary only with depth. It seems to us that studies of detailed inhomogeneous models can be justified only after we have a better understanding of the results that can be obtained by assuming only one spatial coordinate.

In figure 2, we show how our computed intensity spectrum compares with observations of quiet regions near the center of the solar disk in the wavelength region 700–1400 Å. The indicated OSO 4 and OSO 6 data points represent the continuum intensities in narrow spectral windows that appear to be free of emission lines. A summary of the OSO 4 data is given by Dupree and Reeves (1971). The observations of Tousey (1963) are also indicated in figure 2.

We have found not only that the broad wings of Lα have a direct effect on the surrounding spectrum but that, in addition, Lα contributes to the photoionization of carbon and silicon and, hence, influences the carbon and silicon continuum intensities. The problem of the influence of Lα on the spectrum is a difficult one because of uncertainties in the frequency redistribution that takes place when photons are absorbed and reemitted in the line wings. In one test case, we assumed complete frequency redistribution throughout the wings; we found that the computed intensities were much larger than those observed, but that lower temperatures in the region of formation led to disagreement between predicted and observed intensities in other spectral regions. In a second test case, we assumed coherent scattering for Lα every-

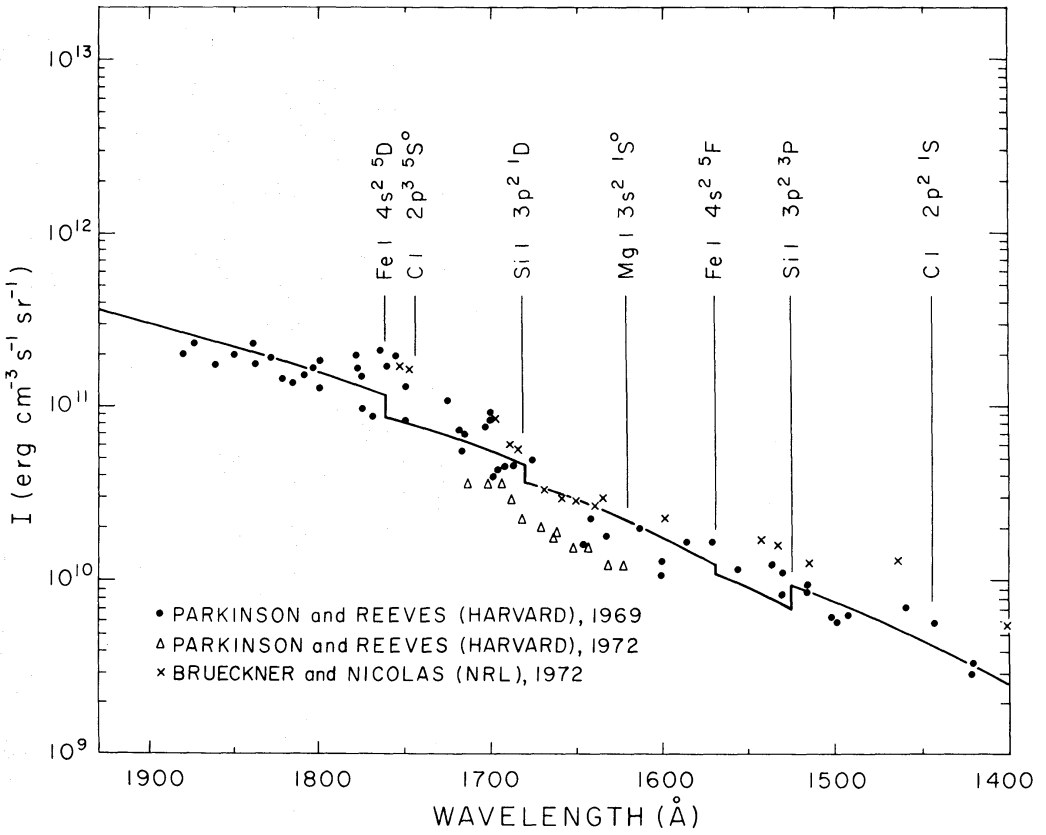

FIG. 3.—Predicted and observed intensities for quiet regions near disk center in the wavelength region 1400–1900 Å. As explained in § XI, an opacity multiplier has been introduced in the region longward of 1682 Å to bring our computed intensities into agreement with the observed values.

where beyond three Doppler widths from line center; we found that the computed wing intensities were much smaller than those observed and that higher temperatures in the region of formation also led to inconsistencies elsewhere. Consequently, we have adjusted the relative proportions of coherent scattering and complete frequency redistribution to obtain the best agreement with observations; this required approximately 93 percent coherent scattering and 7 percent redistribution throughout the line wings. Our analysis of this problem will be presented in a subsequent paper.

Figure 3 compares the computed spectrum between 1400 and 1900 Å with the observations of Parkinson and Reeves (1969, 1972) and of Brueckner and Nicolas (1972). In the wavelength region longward of the silicon edge at 1682 Å, our computed continuous opacity is much smaller than the solar opacity, either because there is a missing continuous opacity or because we do not include the opacity due to line blanketing (or blocking), or a combination of both. The intensity that would be computed with the currently known opacities is formed rather deep in the photosphere and is much greater than the observed intensity (see Gingerich *et al.* 1971, fig. 4). Certain of our photoionization rates depend on computed values of J_ν in this region of the spectrum. In order to avoid errors in these rates, we have increased the opacity longward of 1682 Å by the amount necessary to bring the computed intensity into agreement with observed values. At a given wavelength, the opacity at all depths is multiplied by a constant. This opacity multiplier is 4.0 at 1682 Å, 2.0 at 2000 Å, and unity at 4000 Å; the values at other wavelengths within the range 1682–4000 Å are obtained by linear interpolation. Outside this range, the value is unity.

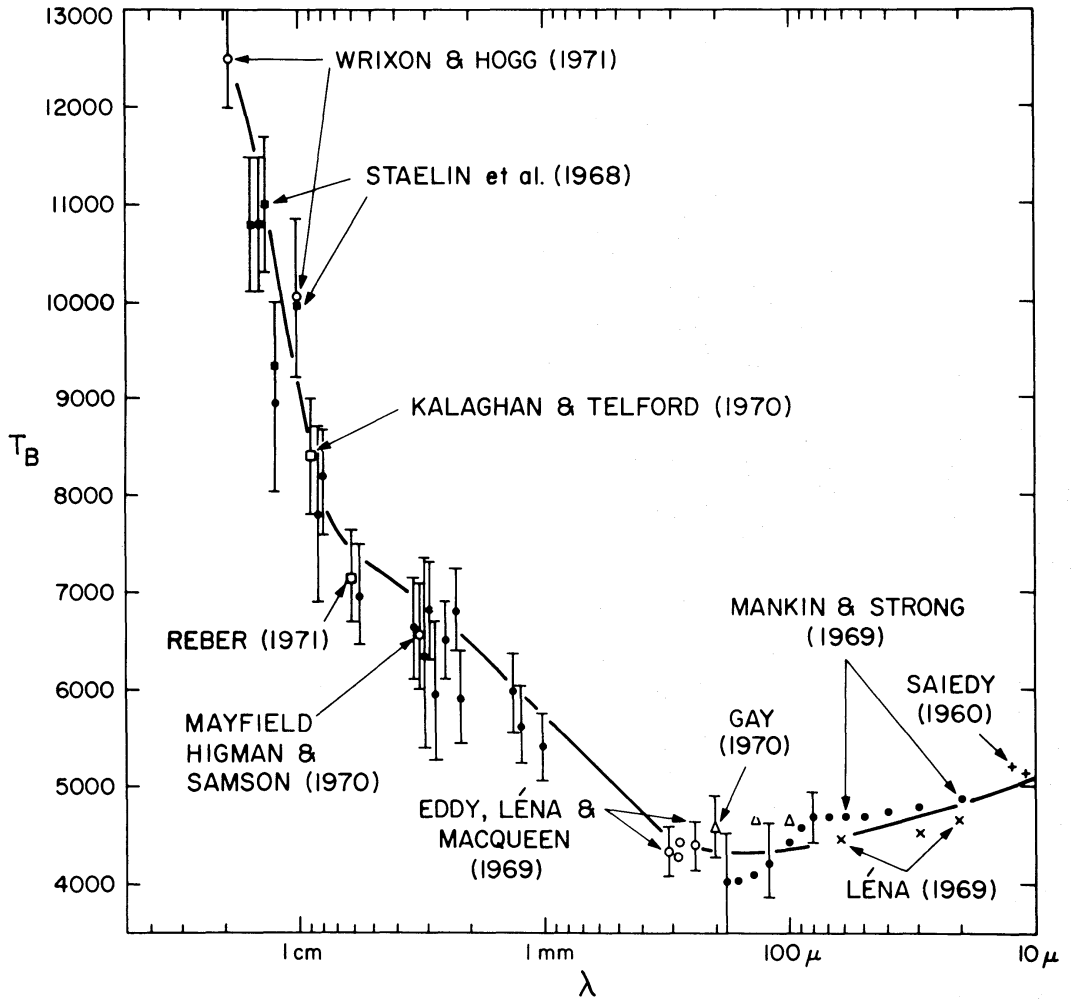

FIG. 4.—Predicted and observed brightness temperatures in the microwave region of the spectrum. References to observations not identified in the figure are given by Linsky and Avrett (1970).

Chromospheric radiation is emitted in the extreme-infrared spectrum as well as in the extreme-ultraviolet. A comparison between our computed brightness temperatures and those observed in the microwave region is shown in figure 4. Observations not identified in this figure are identified in figure 12 of an earlier paper by Linsky and Avrett (1970).

Figure 5 shows the electron density n_e, the total hydrogen density n_H, and the hydrogen ground-state departure coefficient b_1, all plotted as functions of height. In the region out to the chromosphere-corona transition zone, a region in which hydrogen is almost completely neutral, $1/b_1$ is a measure of the degree of hydrogen ionization relative to that computed in LTE (assuming the same temperature and total hydrogen-density distributions in both cases).

The ionized calcium lines and other lines formed in the chromosphere have Doppler widths that exceed purely thermal values. The Doppler width of a line has been given by equation (124), namely,

$$\Delta\lambda_D\,(\text{Å}) = 0.091\,\frac{\lambda\,(\text{Å})}{3000}\left[\frac{1}{M}\,\frac{T}{5000} + \left(\frac{V}{9.1}\right)^2\right]^{1/2}. \qquad (128)$$

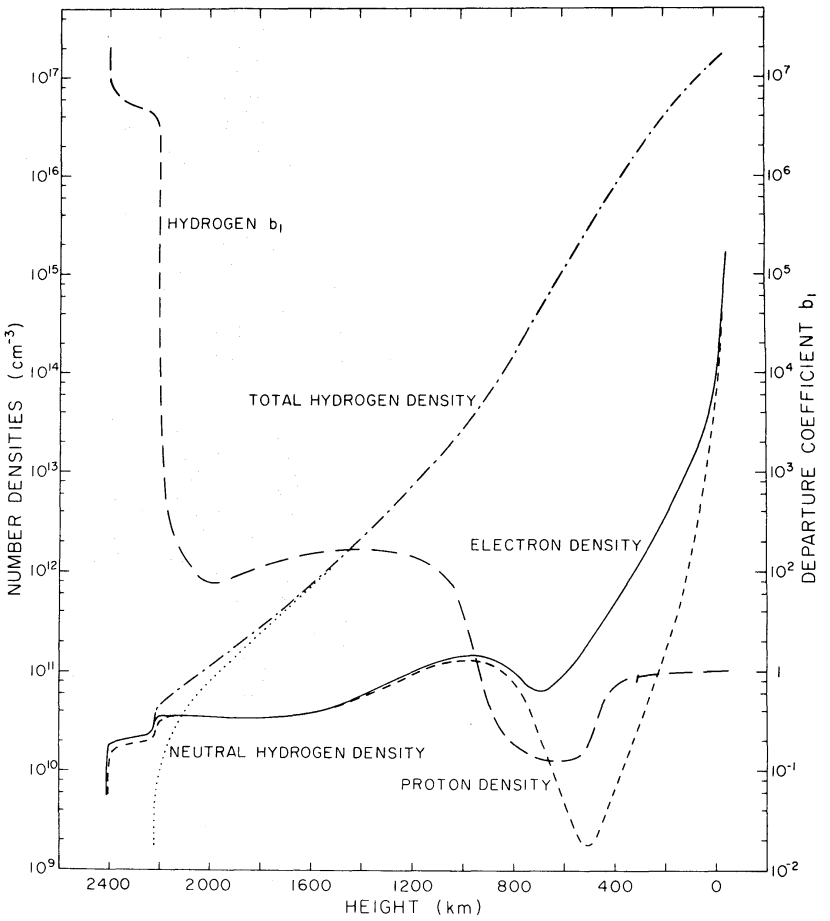

FIG. 5.—The total hydrogen, neutral hydrogen, proton, and electron number densities and the hydrogen ground-state departure coefficient as functions of height.

Our atmospheric model can be used to calculate the profiles of strong and weak lines emitted by atoms of different mass and to determine the various heights and corresponding values of temperature at which these lines are formed. The velocity parameter V is chosen as a function of height in order to increase the calculated Doppler widths to match the observed ones. Line widths observed during an eclipse can also be used to determine V as a function of height above the solar limb.

The results of both the above methods are presented in figure 6. The broken curve represents the velocity distribution adopted by Linsky and Avrett (1970) in order to obtain agreement between observed Ca H, K, and infrared triplet line widths and those calculated by a model similar to the present one. We also indicate the velocities obtained by Hirayama (1971) from line widths observed at eclipse. Hirayama's data are given against height measured above the solar limb. The limb is located near 350 km on our height scale, which has $h = 0$ at radial $\tau_{5000} = 1$. Thus, we have moved the data points 350 km to the left in an attempt to put them on our height scale. Our adopted $V(h)$ is shown as the solid curve. This curve is arbitrary in several respects; we tried to select a simple distribution in general agreement with present observations.

This $V(h)$ is used not only as a contribution to spectral line widths but also as the turbulent-pressure contribution $v_t(h)$ in the hydrostatic-equilibrium equation (see eq. [91]). This contribution leads to an increased scale height (see eq. [93]) and a more gradual pressure decrease with height in the chromosphere. As a result, the sharp

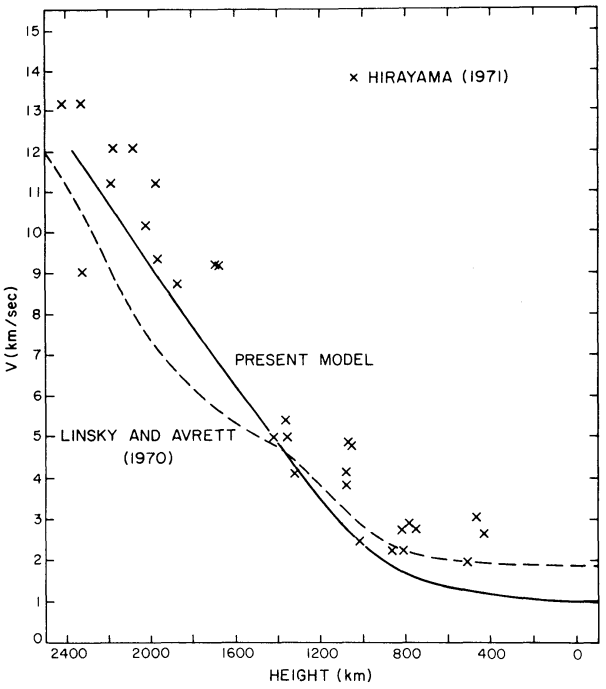

FIG. 6.—The velocity distribution used as a contribution to both line broadening and turbulent pressure. The data points (obtained from line widths at eclipse) were originally given against height measured above the observed limb; they have been moved 350 km to the left to put them approximately on our height scale.

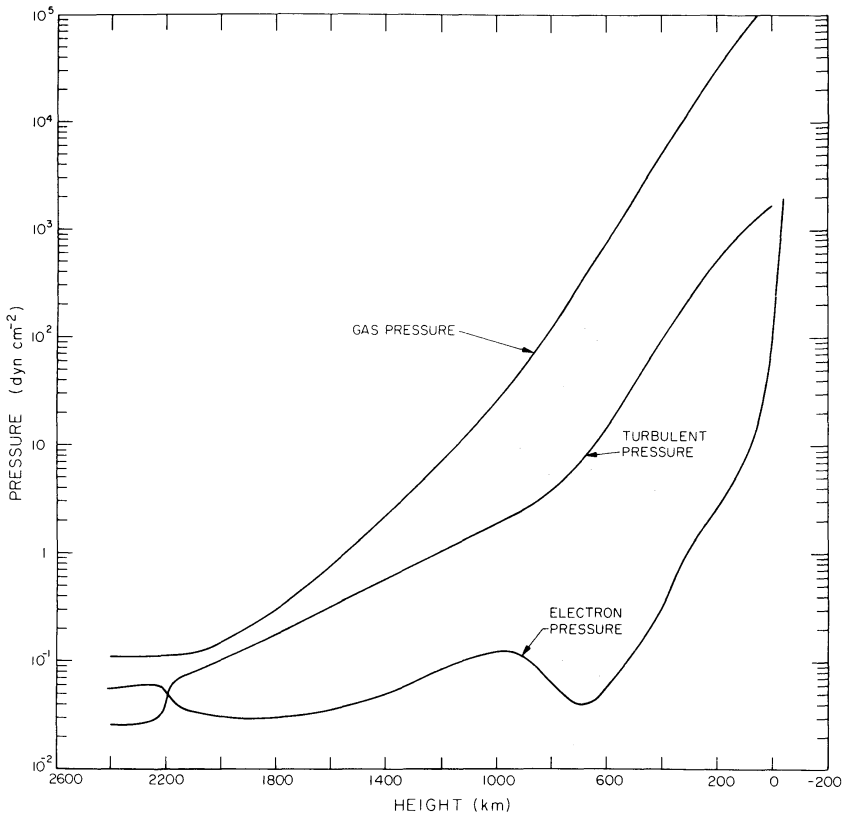

FIG. 7.—The gas pressure, turbulent pressure, and electron pressure as functions of height.

temperature rise in the chromosphere-corona transition zone begins at about 2200 km rather than 1900 km, which would be the result with $v_t(h) = 0$. The larger of these two height values is in better agreement with recent eclipse observations by Makita (1972).

The turbulent pressure corresponding to $v_t(h)$ is generally a small fraction of the gas pressure. Figure 7 shows the gas pressure (eq. [90]), the turbulent pressure $\frac{1}{2}\rho v_t^2$, and the electron pressure $p_e = n_e kT$.

XII. FINAL REMARKS

In this paper, we have described the procedure we use to compute a theoretical solar spectrum. Also, we have given a summary of the results obtained to date. Detailed solutions and comparisons with previous work will be presented in subsequent papers.

Our current chromospheric model is based on solutions of the statistical-equilibrium and radiative-transfer equations for H, H^-, C I, and Si I. In addition, we used the Ca II line widths to determine the broadening velocity variation with height. We have not attempted to adjust the present model to agree with detailed Ca II solutions, because we feel that the assumption of complete frequency redistribution outside the Doppler core of the H and K lines may be invalid, given the results obtained for Lα. These results are summarized in the preceding section.

We are currently solving the transfer and statistical-equilibrium equations for other atoms and ions, particularly He I, He II, Al I, C II, Na I, O I, Fe I, Mg I, and Mg II. An attempt will be made to synthesize the continua and all the prominent absorption and emission lines of these elements. We plan to add many more constituents to our collection of continuous opacity sources in an effort to account properly for the spectrum longward of the silicon discontinuity at 1682 Å.

The immediate purpose of this work is to determine in a semiempirical manner the structure of the solar atmosphere. We have chosen to concentrate first on understanding spectral detail in quiet regions, leaving the matter of active regions and spatial inhomogeneities until later. A detailed knowledge of atmospheric structure allows us to compute radiative and conductive energy transport throughout the atmosphere and to establish detailed constraints on theories of the overall chromospheric energy balance.

Then, perhaps, we can understand the Sun's outer atmosphere well enough to account for the variety of observed solar behavior. Moreover, we can apply this physical understanding and associated diagnostic techniques to the interpretation of other astrophysical phenomena.

We are grateful to Dr. R. W. Noyes for his comments on the manuscript. This research was supported in part by NASA contract NAS 5-9274, NASA grant NGR 22-007-211, and AFCRL contract F 19628-72-C-0054.

REFERENCES

Athay, R. G., and Skumanich, A. 1967, *Ann. d'Ap.*, **30**, 699.
Avrett, E. H. 1968, in *Resonance Lines in Astrophysics* (Boulder, Colo.: National Center for Atmospheric Research), p. 27.
———. 1971, *J. Quant. Spectrosc. and Radiat. Transf.*, **11**, 511.
Avrett, E. H., and Hummer, D. G. 1965, *M.N.R.A.S.*, **130**, 295.
Avrett, E. H., and Loeser, R. 1969, *Smithsonian Ap. Obs. Spec. Rept.*, No. 303.
———. 1973, in preparation.
Browne, J. C., and Dalgarno, A. 1969, *J. Phys. B*, **2**, 885.
Brueckner, G. E., and Nicolas, K. 1972, *Bull. A.A.S.*, **4**, 378.
Chipman, E. G. 1971, *Smithsonian Ap. Obs. Spec. Rept.*, No. 338.
Dupree, A. K., and Reeves, E. M. 1971, *Ap. J.*, **165**, 599.
Eddy, J. A., Léna, P. J., and MacQueen, R. M. 1969, *Solar Phys.*, **10**, 330.
Gay, J. 1970, *Astr. and Ap.*, **6**, 327.
Gebbie, K. B., and Thomas, R. N. 1970, *Ap. J.*, **161**, 229.

Gingerich, O., Noyes, R. W., Kalkofen, W., and Cuny, Y. 1971, *Solar Phys.*, **18**, 347.
Gravila, M. 1967, *Phys. Rev.*, **163**, 147.
Hirayama, T. 1971, *Solar Phys.*, **16**, 384.
Hummer, D. G. 1969, *M.N.R.A.S.*, **145**, 95.
Jefferies, J. T., and White, O. R. 1960, *Ap. J.*, **132**, 767.
Kalaghan, P. M., and Telford, L. E. 1970, Air Force Cambridge Res. Lab. Rept. 70-0052.
Karsas, W. J., and Latter, R. 1961, *Ap. J. Suppl.*, **6**, 167.
Léna, P. J. 1969, *Solar Phys.*, **3**, 28.
Linsky, J. L., and Avrett, E. H. 1970, *Pub. A.S.P.*, **82**, 169.
Makita, M. 1972, *Solar Phys.*, **24**, 59.
Mankin, W. G., and Strong, J. 1969, *Bull. A.A.S.*, **1**, 200.
Mayfield, E. B., Higman, J., and Samson, C. 1970, *Solar Phys.*, **13**, 372.
Menzel, D. H. 1937, *Ap. J.*, **85**, 330.
Menzel, D. H., and Pekeris, G. L. 1935, *M.N.R.A.S.*, **96**, 77.
Noyes, R. W., and Kalkofen, W. 1971, *Solar Phys.*, **15**, 120.
Parkinson, W. H., and Reeves, E. M. 1969, *Solar Phys.*, **10**, 342.
———. 1972, private communication.
Reber, E. E. 1971, *Solar Phys.*, **16**, 75.
Saiedy, F. 1960, *M.N.R.A.S.*, **121**, 483.
Staelin, D. H., Gaunt, N. E., Law, S. E., and Sullivan, W. T. 1968, *Solar Phys.*, **3**, 26.
Thomas, R. N. 1957, *Ap. J.*, **125**, 260.
———. 1960, *ibid.*, **131**, 429.
Tousey, R. 1963, *Space Sci. Rev.*, **2**, 3.
Vernazza, J. E., and Noyes, R. W. 1972, *Solar Phys.*, **22**, 358.
Withbroe, G. L. 1971, in *The Menzel Symposium on Solar Physics, Atomic Spectra, and Gaseous Nebulae*, ed. K. B. Gebbie (NBS Spec. Pub. 353), p. 127.
Wrixon, G. T., and Hogg, D. C. 1971, *Astr. and Ap.*, **10**, 193.